The Simulation and Formability Prediction of a DP600 Steel Reverse Draw - NUMISHEET 2014 Benchmark 1

Changqing Du[1], Kaiping Li[1], Xiaoming Chen[2], Yuzhong Xiao[3], Xinhai Zhu[3]
[1]*Chrysler Group LLC,* [2]*U.S. Steel Corporation,* [3]*LSTC*

Abstract

In this study, the simulation and formability prediction of the DP600 Steel Revers Draw in the NUMISHEET 2014 Benchmark 1 is conducted using LS-DYNA®. The combinations of the material models and element formulations are evaluated for better strain path correlations between the simulation and the measurement at the specified points. Various input factors are considered in this study, including different material model and element type, mesh sizes, integration points and locations. In addition to the conditions given in the benchmark description, extra factors such as the friction effects and springback after drawbead forming process are also considered. The simulation results show that the properly selected yield function is critical for the stain path predictions to be in better agreement with the experimental measurements under such loading condition. In simulation the Formability-Index method is applied to determine the forming limit strains. With this method, the predicted limit strains of the on-set necking points, as well as the locations are compared with the measurement results reported in Benchmark 1 Analysis.

1. Introduction

In this study, the simulation and formability prediction of the DP600 Steel Revers Draw in the NUMISHEET 2014 Benchmark 1 with the full size blank shape of the Shim-4 process are conducted using LS-DYNA.

The combinations of the material models and element formulations are evaluated to find the appropriate selections for better strain path correlations between the simulation and the measurement at the specified points. Then the numerical factors, including the number of the integration points and the element sizes, are also compared. In addition to the recommended conditions in the benchmark description [1], extra factors that may possibly influence the strain path prediction are considered in this study, such as the frictional effects and the drawbead forming process. Since the nonlinear strain paths show noticeable influences on the on-set necking prediction [2-3], the Formability Index (F.I.) [4] method is then applied based on the simulated

strain path results to predict the necking location as well as the limit strains when the on-set necking occurs. The predicted results are compared with the experimental measurement data sets.

2. Simulation procedures

According to the benchmark description [1], the experimental process consists of two steps: the drawbead forming stage and the draw/reverse draw continuous forming stage. Accordingly the simulation procedures are set up in two identical stages:

- Stage 1 – the drawbead forming

The drawbead will be formed on the initially flat blank and the output will be used as the blank in the next stage.

- Stage 2 – the draw/reverse draw continuous forming

With the formed drawbead, the blank will be evenly clamped by the "blank_holder" and the "lower_tool" with the calculated force=407KN, as shown in Fig. 2-1. In this study, the "upper_tool" will move toward the blank while the both of the "lower_tool" "and the "lower_tool_insert" will remain still in the entire process, which is considered to be equivalent to the experiment procedure.

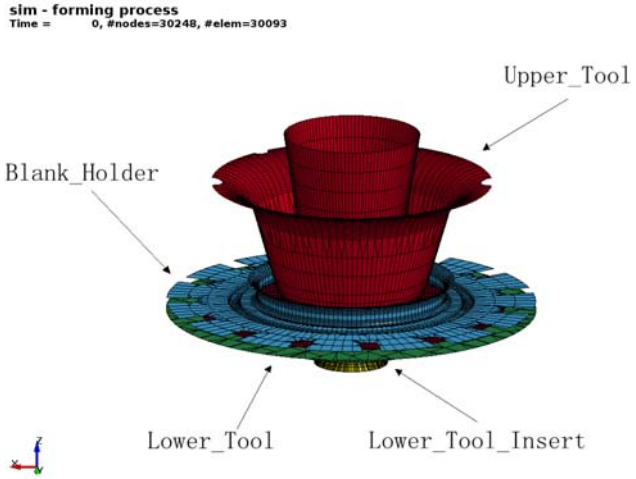

Fig 2-1 The setup of the draw/reverse draw process

According to the benchmark description, the friction effects are not the same between the tools and pre-formed blank: the recommended friction coefficient of the blank holding zones (i.e. the blank_holder vs. the blank) is 0.2 and that of the forming zones (i.e. the lower_tool_insert vs. the blank, and the upper_tool vs. the blank) is 0.02.

3. Comparisons of simulation results and measurements

The simulated strain paths at the specified points on the outer surface where the strains are measured by the Digital Image Correlation system, DIC, are compared

with the measured results of experimental samples as reported in Benchmark 1 Analysis [5].

The experimental measurement data sets of the benchmark include the strain paths of three specified points (Pt-1, Pt-2, and Pt-3, as shown in Fig 3-1), the location and limit strains of the necking point (Pt-4). In the following study, the simulations results will be compared with the experimental data to evaluate the effects of different factors.

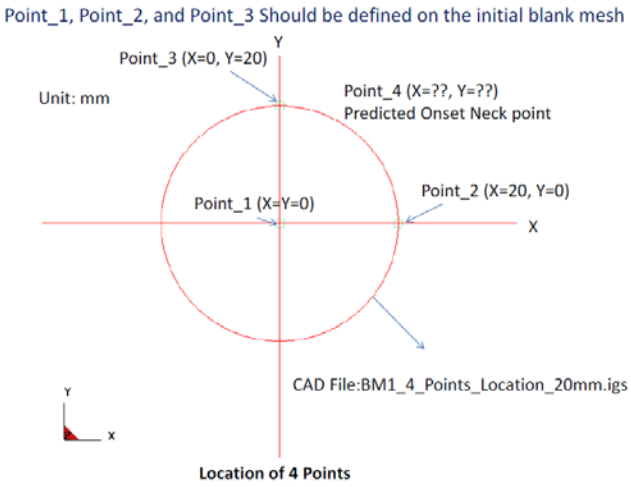

Fig 3-1 The locations of the specified points [1]

3.1 The material models and the element formulations

Throughout the entire process, the zone of interest on the blank does not experience cyclic loading and the isotropic hardening is considered in the simulation. As one of the three materials in the benchmark, the DP600 steel is selected. The full sized blank with the position of the Lower_tool_Insert with 4 shims, Shim-4, as specified in benchmark description is chosen in this study. Swift law is used to describe the stress-strain relationship in the rolling direction. The set of the material constants from the Material Characterization of Benchmark 1 and Benchmark 2 [6] are listed in Table 3-1.

Table 3-1 The R values and constants of the Swift hardening law for DP 600

R_0	R_{45}	R_{90}	K	n	ε_0	Yield stress
0.940	**1.440**	**0.900**	**1097.0**	**0.182**	**0.00192**	**352.3 MPa**

Three commonly used yield functions, MAT_036 (Barlat and Lian 1989), MAT_037 (Hill's 1948 Transversely Anisotropic Elastic Plastic) and MAT_122 (Hill's 1948 planar anisotropy model with 3 R values) [4], are selected to describe the anisotropic properties. Element formulation 16 [7] in LS-DYNA (the Fully Integrated Shell) is chosen along with the above material models.

As shown in Figs 3-2(A), the strain path results of Mat_036 at the high strain zone has the similar trend and is closer to the measured strain path at center of the panel, Pt-1, than MAT_037 and MAT_122 results. At specified Pt-2 and Pt-3, the three material models present similar results as shown in Fig. 3-2(B) and Fig. 3-2(C) respectively.

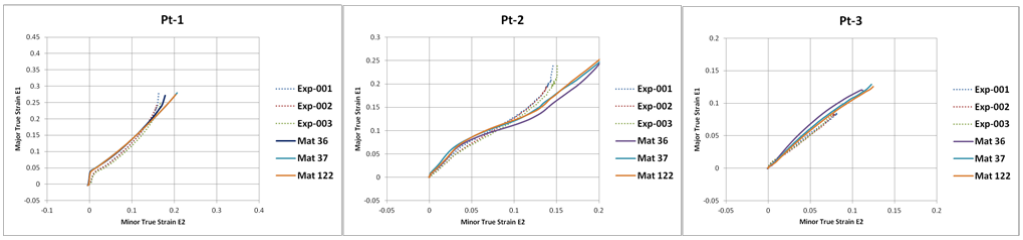

(A) Pt-1 ***(B) Pt-2*** ***(C) Pt-3***

Fig. 3-2 Strain paths comparisons: Measured and simulated using different material models

Based on the results of MAT_036, Element formulation 2 (Belytschko-Lin-Tsay) and 16 (Fully Integrated Shell) [7] are compared. As shown in Fig. 3-3(A-C) no apparent difference is present in the strain paths at the specified points. Although it is possible to switch to Element formulation 2 for the reduced time cost, Element formulation 16 is still recommended due to the existence of the bending deformation.

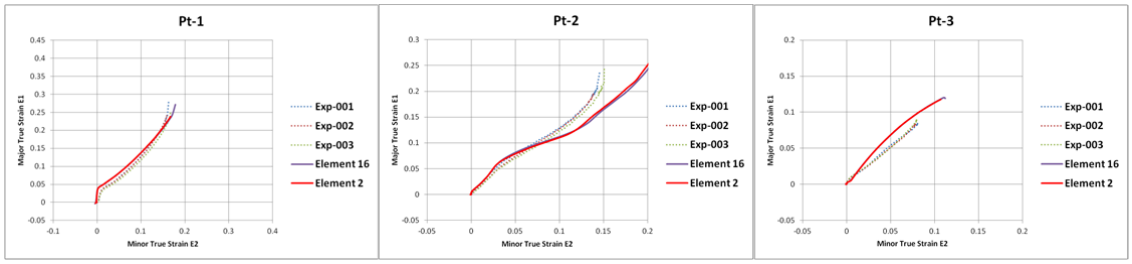

(A) Pt-1 ***(B) Pt-2*** ***(C) Pt-3***

Fig. 3-3 Strain paths comparisons: Measured and simulated using different element formulations

3.2 The integration points and the mesh size effects

Two numbers of the integration points through sheet thickness, 5 and 9, are considered to evaluate whether the accuracy will be increased by the greater number of the integration points. As shown in Fig. 3-4, the simulation results with 5 integration points give the similar strain paths to that with 9 integration points at the specified locations.

To evaluate the influence of the mesh size on the simulation results, the mesh size of 0.5 mm, 1.0 mm and 2.0 mm are considered. With the same element formation 16

and the material model MAT_036, the results of the 2mm mesh size show more discrepancies to the measured strain paths, especially near the necking stage at Pt-1, while those of the 1.0mm and 0.5mm mesh sizes present no significant difference as shown in Fig 3-5.

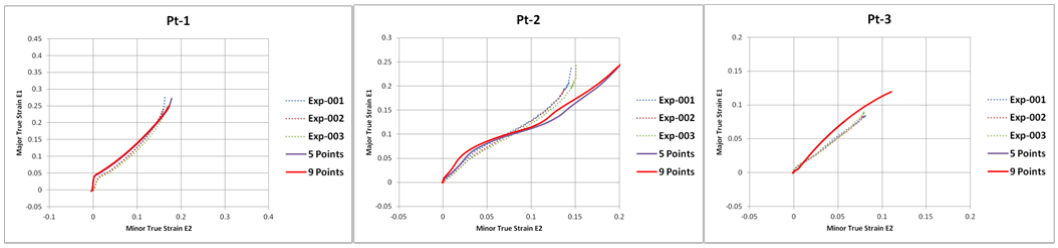

(A) Pt-1 ***(B) Pt-2*** ***(C) Pt-3***

Fig. 3-4 Strain paths comparisons: Measured and simulated using different numbers of the integration points through thickness

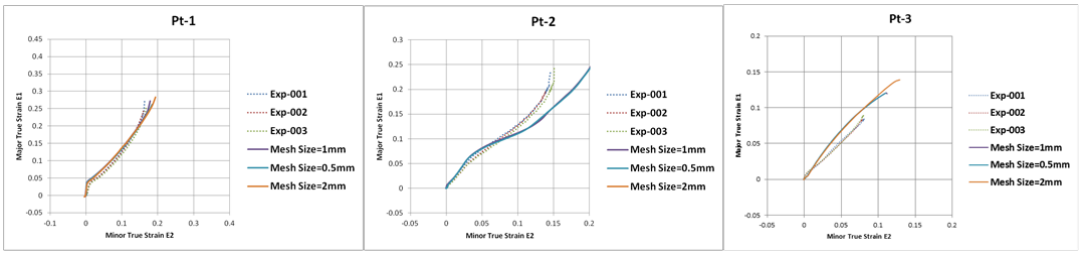

(A) Pt-1 ***(B) Pt-2*** ***(C) Pt-3***

Fig. 3-5 Strain paths comparisons: Measured and simulated using different mesh sizes

3.3 The friction coefficient effects

The above analyses are based on the recommended conditions of the benchmark. More factors with possible influences on the simulation results have been studied according to the detailed description of the actual experimental procedure [1].

As indicated in the experiment description, in the low friction area (i.e. between the Lower_Tool_Insert and the blank, and the Upper_Tool and the blank), the tools do not directly contact the blank but they are in fact separated by the chemistry gloves, which can undertake severe shear deformation with very small elastic modulus as 0.00028 MPa. Thus the reaction between the tool and the blank is equivalent to a frictional contact condition with greatly reduced friction coefficient. In order to evaluate the friction coefficient effects two more friction coefficients (0.002, 0.05) are simulated in addition to the suggested value, 0.02, in the detailed description of the actual experimental procedure [1]. As show in Figs 3-6 (A), The results of friction coefficient, 0.02, for both upper and lower tool sheet contact interfaces with chemistry gloves, shows better correlation of the strain path of Pt-1 at the high strain end with the experimental results. The value 0.02 is applied in further simulation models.

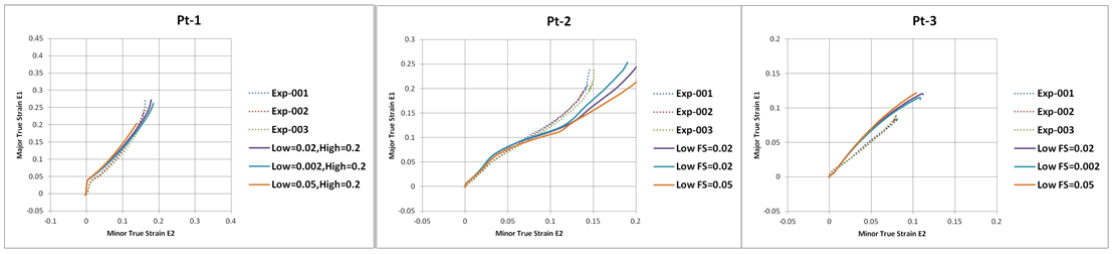

(A) Pt-1 *(B) Pt-2* *(C) Pt-3*

Fig. 3-6 Strain paths comparisons: Measured and simulated using different friction coefficients

3.4 The influence of springback after the draw-bead forming process

As suggested in the benchmark description, an alternative of the simulation procedure can be considered by incorporating the springback of the blank after the drawbead forming process. Although the strain of the blank after the forming of the drawbead is assumed to be negligible, the initial geometry of blank for Stage 2 may still have influence on the final strain path prediction. In addition, the drawbead of the binder in Stage 2 are not identical to those in Stage 1 as indicated in the benchmark description. The simulations with the sprung blank shape after the Stage 1 process may affect the results of Stage 2. In this study the output of the sprung shape of Stage 1 with the initial strain and stress is used as the blank in Stage 2 simulation. In this case, 9 integration points are used in the bead forming process, the springback after bead forming process, Stage 1, and the draw/reverse draw process, Stage 2, to capture through-thickness stress distributions.

As shown in Fig. 3-7, incorporating the springback process has no apparent influence on the strain path of Pt-1 in this case, while some improvement in the strain path of Pt-2 can be noted.

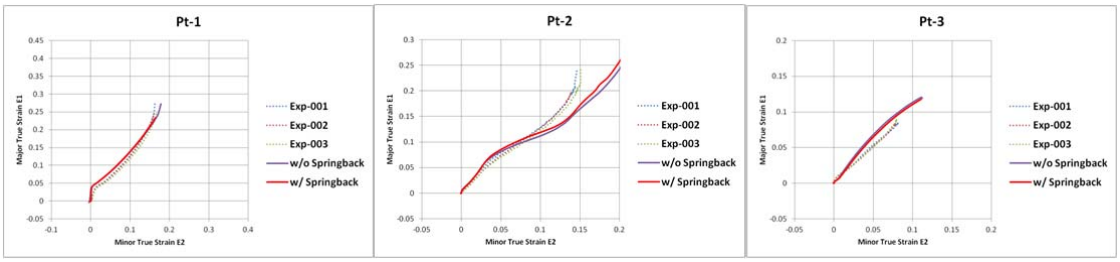

(A) Pt-1 *(B) Pt-2* *(C) Pt-3*

Fig. 3-7 Strain paths comparisons: Measured and simulated with and without the springback process

4. The on-set necking prediction with the Formability Index method

The Formability Index (F.I.) for the DP600 steel is developed based on the provided linear strain path Forming Limit Curve (FLC) of DP600 [6] as descripted in references [2] and [3].

In the on-set necking strain simulations the basic setup as listed in Table 4-1 is applied. Based on strain history results of the simulations, the F.I. method is used to determine the location of the first necked point and when the on-set necking occurs.

Table 4-1 Basic Simulation setup

Label	Material model	Element formulation	Integration points	Mesh size(mm)	Friction coefficient
Standard	Mat 36	16	5	1	0.02
w/ Springback	Mat 36	16	9	1	0.02

The comparisons of on-set necking locations and the strains between the measured experimental samples and the F.I. predictions on simulation results are listed in Table 4-2 and shown in Fig. 4-1.

The predicted on-set necking location is within the measurement range of three experiments. It should be noted that although the discrepancies of strain paths between the simulated and experiments can be observed from Fig. 4-1, the on-set necking strains of the prediction correlate well with the measurements: The average of the measured on-set necking strains of the three experiments is about 0.065 below the given linear strain path Forming Limit Curve (FLC) of DP600; the strains of F.I. prediction on the upper surface, which is the same side of measured surfaces of the experimental samples, is about 0.062 below the FLC.

Table 4-2 The predicted location point and its necking limit strains

	X (mm)	Y (mm)	E1	E2
EXP-001	**10.3209**	**0**	**0.2746**	**0.1883**
EXP-002	**13.3339**	**0**	**0.2596**	**0.1835**
EXP-003	**13.7658**	**0**	**0.2596**	**0.1866**
EXP-Average	**12.4735**	**0**	**0.2616**	**0.1861**
Sim-Upper	**12.5**	**0**	**0.2884**	**0.2083**
Sim-Middle	**12.5**	**0**	**0.3208**	**0.2250**
Sim-Lower	**12.5**	**0**	**0.3302**	**0.2294**

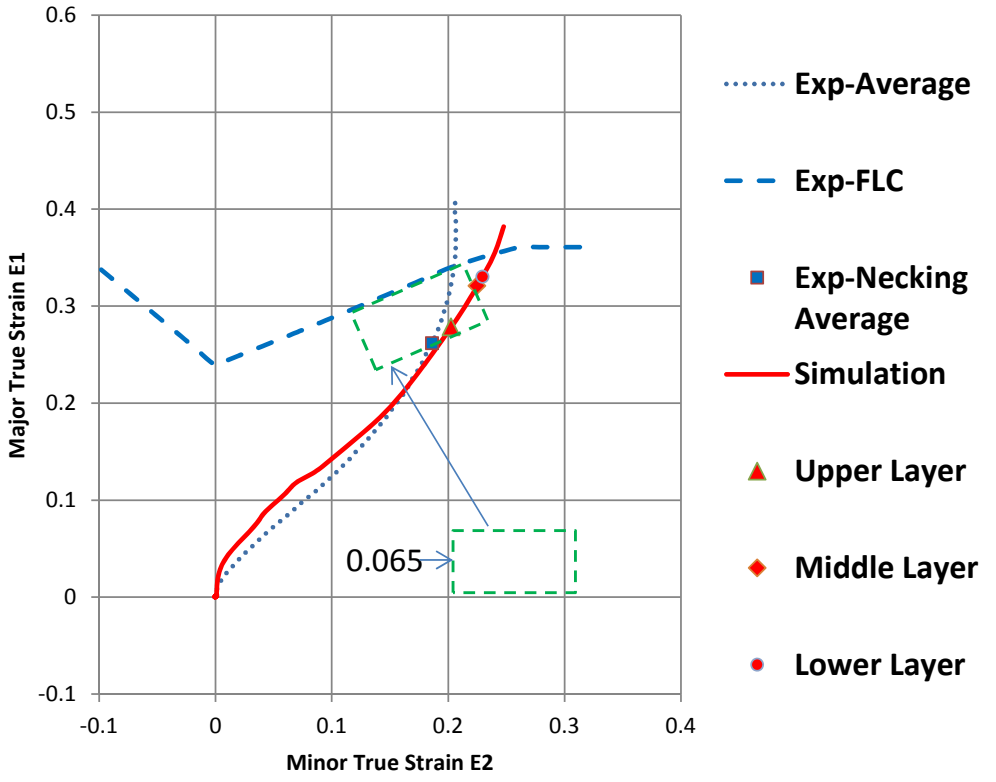

Fig. 4-1 On-set necking comparison: Measured and F.I on the Simulated Strain Path

5. Summary

With the given conditions in the benchmark, the effects of various factors, including different material models, element formulations, mesh sizes, and the integration points, have been evaluated. In addition, extra factors such as the friction effects and the springback after drawbead forming process were also investigated.

The simulation results show that the strain path result of Mat_036 (Barlat and Lian 1989) at the high strain zone has the similar trend and is closer to the measured strain path at center of the panel than other two studied material models. The mesh size should be limited to 1mm. Other factors such as the location and number of integration show no apparent influence on the strain path results. The provided friction coefficient for the tool and sheet contact interfaces with the chemical gloves is reasonably good. The simulations with the drawbead forming process show minor influence in the strain path predictions. The applied Formability Index, F.I., method has predicted the on-set necking locations and strains with good correlations with the measurements on the experimental samples of the Reverse Draw of Benchmark 1.

References

[1] Benchmark Committee, Benchmark 1 – Nonlinear Strain Path Forming Limit of a Reverse Draw: Part A: Benchmark Description. AIP Conference Proceedings, Volume 1567, NUMISHEET 2014.

[2] T.B. Stoughton, X. Zhu. Review of Theoretical Models of the Strain-Based FLD and their Relevance to the Stress-Based FLD, International Journal of Plasticity", V. 20, Issues 8-9, P. 1463-1486, 2003.

[3] D. Zeng, X. Zhu, L. B. Chappuis, Z. C. Xia, "A Path Independent Forming Limited Criterion for Sheet Metal Forming Simulations", 2008 SAE Proceedings, Detroit MI, April, 2008.

[4] Livermore Software Technology Corporation, "LS-DYNA Keyword User's Manual, Version 971", Volume II.

[5] X. Wu, "Benchmark 1 –Nonlinear Strain Path Forming Limit of a Reverse Draw-Part C: Benchmark Analysis", AIP Conference Proceedings, Volume 1567, NUMISHEET 2014, P.39, 2014.

[6] Thomas B. Stoughton, Ming F. Shi, Gang Huang, and Jeong Whan Yoon, "Material characterizations for Benchmark 1 and Benchmark 2", AIP Conference Proceedings, Volume 1567, NUMISHEET 2014, P.9, 2014.

[7] Livermore Software Technology Corporation, "LS-DYNA Keyword User's Manual, Version 971", Volume I.